Ion-size effect at the surface of a silica hydrosol

Aleksey M. Tikhonov[a)]
P. L. Kapitza Institute for Physical Problems, RAS, Kosygina 2, Moscow 119334, Russia

(Received 24 April 2008; accepted 3 December 2008; published online 14 January 2009)

Using synchrotron x-ray reflectivity, I studied the ion-size effect for alkali ions (Na^+, K^+, Rb^+, and Cs^+), with densities as high as 4×10^{18}–7×10^{18} m^{-2}, suspended above the surface of a colloidal solution of silica nanoparticles in the field generated by the surface electric-double layer. I found that large alkali ions preferentially accumulate and replace smaller ones at the surface of the hydrosol, a result qualitatively agreeing with the dependence of the Kharkats–Ulstrup single-ion electrostatic free energy on the ion's radius. © *2009 American Institute of Physics*.
[DOI: 10.1063/1.3056663]

The participation of small inorganic ions in a variety of surface phenomena at air-liquid and liquid-liquid interfaces is of practical significance in many applications.[1–3] Numerous authors have discussed the ionic distributions, surface tension, image forces, and single-ion free energy at the surface of an electrolyte solution.[4–15] For decades, molecular-dynamics simulations were used extensively to explore molecular structure and ion-specific effects at liquid surfaces.[16–18] However, synchrotron x-ray scattering is proving particularly valuable as it offers information about the structure of the liquid surface at the microscopic level, giving details that cannot be acquired by measuring macroscopic characteristics, such as surface tension, interfacial capacitance, and surface potential.[19–29] In this paper, I discuss my findings using synchrotron x-ray reflectivity to elucidate the ion-size effect for alkali ions (Na^+, K^+, Rb^+, and Cs^+) elevated above the surface of a colloidal solution of silica nanoparticles by the field of the surface electric-double layer.

The traditional Wagner–Onsager–Samaras approximation treats ions as point charges.[8,9] However, the major difficulty of this approach concerns the divergence of the free energy of a point charge at a flat interface between two dielectric media. Kharkats and Ulstrup[10] resolved this problem by assuming that the ion has a nonzero size. Accordingly, in a continuous media approximation, the following is the free energy $F(z)$ of a spherical charge q with radius a at the boundary between two dielectric media imbedded within a spherical cavity,

$$F(0\le z\le a)=\frac{q^2}{32\pi\varepsilon_0\varepsilon_2 a}\left[2+\frac{2z}{a}+\left(\frac{\varepsilon_2-\varepsilon_1}{\varepsilon_1+\varepsilon_2}\right)\left(4-\frac{2z}{a}\right)+\left(\frac{\varepsilon_2-\varepsilon_1}{\varepsilon_1+\varepsilon_2}\right)^2\left(\frac{(1-z/a)(1-2z/a)}{1+2z/a}+\frac{a}{2z}\ln\left\{1+\frac{2z}{a}\right\}\right)\right]+\frac{q^2}{16\pi\varepsilon_0\varepsilon_1 a}\left(\frac{2\varepsilon_1}{\varepsilon_1+\varepsilon_2}\right)^2\left(1-\frac{z}{a}\right) \quad (1)$$

and

$$F(z\ge a)=\frac{q^2}{32\pi\varepsilon_0\varepsilon_2 a}\left[4+\left(\frac{\varepsilon_2-\varepsilon_1}{\varepsilon_1+\varepsilon_2}\right)\frac{2a}{z}+\left(\frac{\varepsilon_2-\varepsilon_1}{\varepsilon_1+\varepsilon_2}\right)^2\left(\frac{2}{1-(2z/a)^2}+\frac{a}{2z}\ln\left\{\frac{2z+a}{2z-a}\right\}\right)\right], \quad (2)$$

where ε_0 is the dielectric permittivity of the vacuum and ε_1 and ε_2 are the dielectric permittivities of the bottom (water $\varepsilon_1\approx80$) and top (air $\varepsilon_2\approx1$) phases, respectively; the z-axis is directed normal to the surface (oriented by gravity) toward the top phase. The electrostatic free energy of the ion in the water ($z\le0$) is obtained from Eqs. (1) and (2) by exchanging $\varepsilon_1\Leftrightarrow\varepsilon_2$. Several authors revised and discussed Eqs. (1) and (2).[12,14,16] For example, Markin and Volkov[14] used them to explain the dependence of the surface tension of aqueous electrolyte solutions on ionic radii.

In general, an alkali ion in aqueous media is repelled from the surface of water (toward the water's bulk) by its electrical image. The thickness of the transition layer at the surface of a concentrated aqueous solution of a simple inorganic ionic salt (for example, CsCl) is less than 1 nm.[28] However, the larger the radius of an ion, the weaker is its interaction with the boundary, although this feature is important only in the very narrow interfacial region, $\sim2a$, i.e., about as wide as the size of the ion above the surface of water [Fig. 1(a)]. At a distance of several ion radii from the surface, the ion interacts with the boundary as a point charge. For the Na^+ radius, $a\approx1.2$ Å, for K^+ $a\approx1.5$ Å, for Rb^+ $a\approx1.7$ Å, and for Cs^+ $a\approx1.8$ Å.[30,31]

The solid lines in Fig. 1(b) depict the deviation, at the air-water interface, of the single-ion Kharkats–Ulstrup free energies $F_M(z)$ of these monovalent alkali ions M^+(=K^+, Rb^+, Cs^+) from the energy of Na^+, $F_{Na}(z)$; the dot-dashed line represents the difference between $F_{Cs}(z)$ and $F_K(z)$. On the one hand, at $z<0$ $\Delta F<0.03$ eV ($\sim k_BT$ at $T=298$ K and k_B is Boltzmann's constant) is small, featureless, and associated mostly with the difference in the Born solvation energies, $F_M(-\infty)$, of the ions in water. On the other hand, at $z\ge0$, these curves display minima as deep as

[a)]Electronic mail: tikhonov@kapitza.ras.ru.

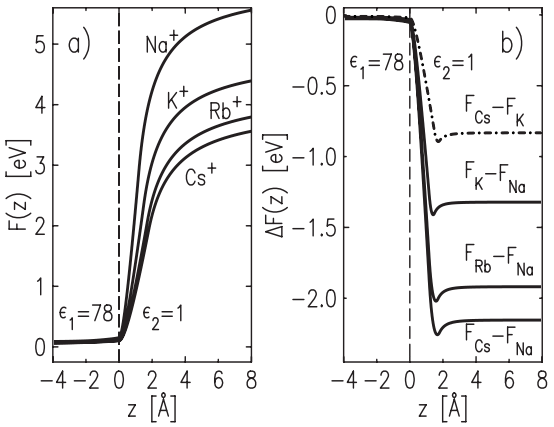

FIG. 1. Kharkats–Ulstrup size effect at the air-water interface: (a) Single-ion electrostatic free energy of the alkali ions at the air-water interface as a function of z; (b) differences between free energies $F_M(z)$ of monovalent alkali ions (M=Na,K,Rb,Cs) at the air-water interface. For Na^+ the radius $a \approx 1.2$ Å for K^+ $a \approx 1.5$ Å, for Rb^+ $a \approx 1.7$ Å, and for Cs^+ $a \approx 1.8$ Å (Refs. 30 and 31).

0.05–0.1 eV ($2k_BT$–$4k_BT$) at ~2 Å above the surface of the water: hence, larger alkali ions preferentially accumulate there, replacing smaller ones (ion-size effect). Usually, this effect is unimportant at room temperature because, for example, the elevation of $Na^+ \sim 1$ Å above the surface of the water is associated with a significant energy barrier of ~2.5 eV; overcoming it would require very specific boundary conditions, viz., an interfacial electric field $>10^9$ V/m. A field of such strength, which cannot be realized in an electrolytic capacitor, is common at the surface of a silica hydrosol that is polarized strongly by the forces of electrical imaging.[32,33]

A four-layer model can describe the structure of the surface of a hydrosol according to x-ray reflectivity and grazing-incidence diffraction data for NaOH-stabilized and Cs-enriched suspensions with monodispersed 5, 7, and 22 nm silica particles (Fig. 2).[32–35] The top two layers in Fig. 2 reflect the adsorption of alkali ions, i.e., a low-density layer (1) of suspended (elevated) ions and a layer (2) of space charge with a surface density of Na^+ $\Phi_{Na} \approx 8 \times 10^{18}$ m^{-2}. The former is inhabited either by Na^+ and/or Cs^+ ions, depending on the bulk concentration of cesium, c^+_{Cs}, in the hydrosol, with roughly one water molecule per ion. On the

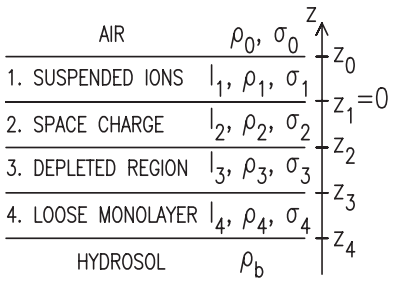

FIG. 2. The four-layer slab model of hydrosol's surface-normal structure. Each layer has a thickness l_m and an electron density ρ_m. In addition, σ_m parameters determine the interfacial width between slabs of electron density (the standard deviation of their locations z_m). At $q_z > 0.1$ Å^{-1} only three interfaces (top two layers with adsorbed ions) contribute to the reflectivity since $\sigma_3 \sim \sigma_4 \gg \sigma_0, \sigma_1, \sigma_2$. The density ρ_1 is the only parameter of the surface-normal structure that depends strongly on the composition of the alkali metal.

contrary, the space-charge layer forms by the hydrated ions with ten H_2O molecules per alkali ion. The depleted layer (3) with a low concentration of electrolytes (~10–20 nm thick) separates these layers from the anionic colloidal particles: its density roughly equals that of the density of bulk water under normal conditions, ρ_w(=0.333 $e^-/Å^3$). Finally, the thickness of layer 4 is the same as the diameter of the colloidal nanoparticles in the sol; the concentration of particles in the loose monolayer is up to twice as high as in the bulk.

The pronounced width of the transition region (~20–50 nm) at the hydrosol's surface reflects the extremely large difference between the forces of electrical imaging for nanoparticles and the monovalent alkali ions. In fact, it is comparable to the Debye screening length in the solution, $\Lambda_D = \sqrt{\varepsilon_0 \varepsilon_1 k_B T/(c^- N_A e^2)} \approx 10-100$ nm, wherein N_A is the Avogadro constant, e is the elementary charge, and c^- is the bulk OH^- concentration ($c^- \approx 10^{-3}-10^{-5}$ mol/l at pH =9–11).

With increasing c^+_{Cs}, the density of layer 1 rises (Cs^+ replaces Na^+ in the layer) and then saturates ($c^+_{Cs} > 0.1-0.2$ mol/l), so that for Cs-enriched sols with 5, 7, and 22 nm particles the reported surface density of Cs^+ in layer 1 were the same, and reached as high as $\Theta_{Cs} \approx 3 \times 10^{18}$ m^{-2}. Dissimilarly, the densities of the layers 2–4 virtually do not depend on c^+_{Cs}. Here, Fig. 1 is valid only quantitatively for the surface of the hydrosol, since at the surface charge density $\Phi_{Na} e \sim 1$ C/m^2 the dialectic permittivity of "surface water" should be very small, $\varepsilon_1 \sim 3$ (see, Fig. 1 in Ref. 36). The strength of the electric field (normal to the surface) of space-charge layer 2, supporting the elevated ions in layer 1, is as high as $\sim \Phi_{Na} e/\varepsilon_0 \varepsilon_1 \sim 10^{10}$ V/m. Hence, in the Kharkats–Ulstrup theory, the effect of the preferable adsorption of Cs^+ in layer 1 can be considered as a manifestation of the ion-size effect of the suspended ions.

I systematically studied the effects on the density of layer 1 at the surfaces of monodispersed suspensions of 22 nm silica particles enriched by different alkali ions (K^+, Rb^+, Cs^+). To ensure that layer 1 was saturated, I chose a bulk concentration of alkali metals, c^+, in the hydrosols that was significantly larger than the concentration of sodium ($c^+ \gg c^+_{Na} \approx 0.06$ mol/l). The solutions were prepared, following Ref. 34, by mixing, either mechanically or ultrasonically (Branson 2510), a 1:1 (by weight) solution of alkali-metal hydroxide MOH in de-ionized water (Barnstead UV), with an NaOH-stabilized sol of 22 nm silica particles (~30% of SiO_2 by weight).[37] The total concentration of alkali in the sol ranged from 0.7 to 0.9 mol/l.[38] I selected the size of silica particles in the hydrosol specifically to facilitate my interpretation of the x-ray reflectivity data: the larger the particles, the smaller their contribution to reflectivity at high incident angles. This relationship is apparent both in the wide surface-normal structure of the 22 nm particle's sol and the high surface roughness of the loose monolayer (Fig. 2). At room temperature, these suspensions (pH < 11.5) remain liquid in a closed container for at least one month.

I carried out all x-ray reflectivity measurements at beamline X19C, the National Synchrotron Light Source, Brookhaven National Laboratory, employing a monochromatic focused x-ray beam ($\lambda = 0.825 \pm 0.002$ Å).[39] Liquid

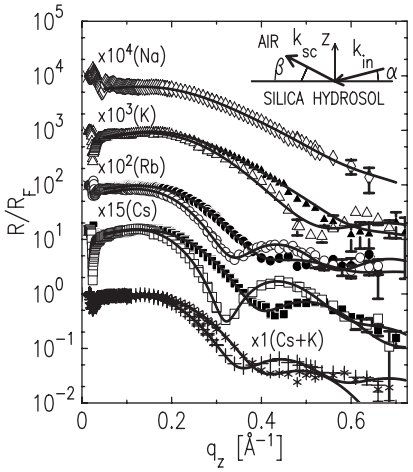

FIG. 3. The surface-structure factors of the 22 nm particle sols: The rhombi represent sol stabilized by NaOH, $c^+_{Na}\approx 0.1$ mol/l; the filled and open triangles are for potassium-enriched sols with $c^+_K\approx 0.8$ mol/l and $c^+_{Na}\approx 0.06$ mol/l; the dots and circles are for rubidium-enriched sols with $c^+_{Rb}\approx 0.6$ mol/l and $c^+_{Na}\approx 0.06$ mol/l; the filled and open squares are for cesium-enriched sols with $c^+_{Cs}\approx 0.7$ mol/l and $c^+_{Na}\approx 0.06$ mol/l. Here, filled and open symbols on each R/R_F curves refer to samples with different equilibration histories. The crosses and stars are for mixtures of cesium- and potassium-enriched sols with $c^+_K\approx 0.4$ mol/l, $c^+_{Cs}\approx 0.3$ mol/l, and $c^+_{Na}\approx 0.06$ mol/l. The lines denote the first Born approximation that is discussed in the text. Insert: $\mathbf{k}_{in}$ and $\mathbf{k}_{sc}$ are, respectively, wave vectors of the incident beam, and the beam scattered toward the point of observation, and $\mathbf{q}$ is the wave-vector transfer, $\mathbf{q}=\mathbf{k}_{in}-\mathbf{k}_{sc}$. At reflectivity conditions ($\alpha=\beta$) there is only one component of the wave-vector transfer, $q_z=(4\pi/\lambda)\sin(\alpha)$, where α and β are the angles of the incident and scattered beams in the plane normal to the surface. The reflectivity was measured with the detector's vertical slit gap of ~0.8 mm at the distance of ~700 mm form the footprint or angular acceptance at $\Delta\beta=6.8\times 10^{-2\circ}$ (twice higher than in Ref. 34) and its horizontal acceptance at ~0.8° (~10 mm gap).

samples with a planar surface were studied in a ~50 ml Teflon dish, 100 mm diameter circular interfacial area, placed inside an air-tight single-stage thermostat and mounted above the level of water in a bath (~200 mm diameter). The bath served as a humidifier in the thermostat. Normally, the samples were equilibrated at $T=298$ K for at least 12 h. Reflectivity was measured with the detector's vertical angular acceptance at $\Delta\beta=6.8\times 10^{-2\circ}$ (twice as high than in Ref. 34) and its horizontal acceptance at ~0.8°.

Figure 3 shows x-ray surface reflectivity $R(q_z)$ of the sols as a function of wave-vector transfer, $q_z=(4\pi/\lambda)\sin(\alpha)$, where α is an incident angle (see insert in Fig. 3). They are normalized to the Fresnel function $R_F(q_z)$, that is, the reflectivity from a sharp surface with no structure. The structure factor $R(q_z)/R_F(q_z)$ consists of two parts: The low q_z-part ($q_z<0.05$ Å^{-1}) is associated with a surface-normal distribution of nanoparticles and, at $q_z>0.1$ Å^{-1}, the surface-normal structure depends strongly on the alkali-metal composition of the sols. The oscillations of reflectivity at $q_z>0.1$ Å^{-1} depend on the sample's equilibration history; usually, they were stronger when the hydrosol's temperature was ~30 K (at $p\mathrm{H}\sim 13$) higher than the room temperature at the beginning of equilibration (open symbols in Fig. 3). This effect probably is due to the narrowing of the surface-electric-double layer at $p\mathrm{H}\sim 13$, so that more alkali ions are available for adsorption (in the equilibrium $p\mathrm{H}<11.5$). Once the sample had equilibrated in the thermostat, for several days thereafter the reflectivity curves were reproducible within the error bars.

Both Parratt formalism (see Ref. 34 for details) and the first Born approximation were used to obtain information about the distribution of adsorbed ions from the x-ray reflectivity values.[40–42] The former also generates data about the surface-normal distribution of nanoparticles from the reflectivity near the angle of total reflection of the surface of a hydrosol, α_c. However, when multiphoton scattering is unimportant (usually at $\alpha>3\alpha_c$) the first Born approximation relates reflectivity to the electron-density gradient normal to the interface, $\langle d\rho(z)/dz\rangle$, averaged over the interfacial plane as the following:

$$\frac{R(q_z)}{R_F(q_z)}\approx\left|\frac{1}{\rho_b}\int_{+\infty}^{-\infty}\left\langle\frac{d\rho(z)}{dz}\right\rangle\exp(iq_z z)dz\right|^2, \qquad (3)$$

where $R_F(q_z)\approx(q_z-[q_z^2-q_c^2]^{1/2})^2/(q_z+[q_z^2-q_c^2]^{1/2})^2$ is slightly different for each sol since $q_c\approx(4\pi/\lambda)\alpha_c$ is defined by the angle of total reflection $\alpha_c=\lambda\sqrt{r_e\rho_b/\pi}\approx 0.09°$ and $r_e=2.814\times 10^{-5}$ Å is the electron's Thomson's scattering length. The bulk electron densities of the sols, ρ_b, are established from their densities and known chemical compositions (Table I).

At $q_z>0.1$ Å^{-1}, only three interfaces (the top two layers with adsorbed ions) contribute to reflectivity since $\sigma_3\sim\sigma_4>30$ Å (see Ref. 34). Then, for the slab model (Fig. 2) with

TABLE I. Estimates of the model parameters in Eq. (4) (see also Fig. 2). c^+_{Na} is the bulk concentration of sodium in the hydrosols; c^+_M is the bulk concentration of alkali ions M^+ (M=K,Rb,Cs) in the enriched sols; l_i are the thicknesses of the interfacial layers with electron densities ρ_i/ρ_w, normalized to the density of bulk water under normal conditions ($\rho_w=0.333$ e$^-$/Å^3); $\sigma_0=\sigma_1=\sigma_2=\sigma$. Parameters l_1 and ρ_1/ρ_w in the rows shifted upward and downward correspond, respectively, to the data in Fig. 3 shown by the open and solid symbols. The bulk electron densities of the sols, ρ_b, were established from their densities and known chemical compositions. The error bars were estimated utilizing the conventional χ^2-criteria at the confidence level of 0.95.

c^+_{Na} (mol/l)	c^+_M (mol/l)	ρ_b/ρ_w	l_1 (Å)	l_2 (Å)	ρ_1/ρ_w	ρ_2/ρ_w	ρ_3/ρ_w	σ (Å)
0.1	–	1.33	8 ± 1	11 ± 1	0.2 ± 0.05	1.20+0.08/−0.01	1.00 ± 0.01	2.8 ± 0.2
			7.0 ± 0.5		0.29+0.03/−0.04			
0.06	0.8 (K^+)	1.21	7.0 ± 0.5	11 ± 1	0.26+0.06/−0.09	1.26+0.02/−0.04	0.99 ± 0.03	2.7 ± 0.3
			7.7 ± 0.5		0.84+0.05/−0.04			
0.06	0.6(Rb^+)	1.24	7.6 ± 0.5	11.8 ± 0.5	0.51+0.05/−0.07	1.30+0.04/−0.03	1.07 ± 0.03	2.7 ± 0.2
			9.0 ± 0.3		0.93 ± 0.04			
0.06	0.7(Cs^+)	1.24	6.5 ± 0.4	11.4 ± 0.5	0.90 ± 0.04	1.31 ± 0.04	1.05 ± 0.05	2.8 ± 0.3

symmetrical error-function profiles of electron density across the interfaces, the structure factor can be reduced to the following simple equation:[43–46]

$$\frac{R(q_z)}{R_F(q_z)} \approx F(q_z)\exp(-\sigma^2 q_z^2),$$
$$F(q_z) = \frac{1}{\rho_b^2}\left|\sum_{m=0}^{2}(\rho_m - \rho_{m+1})\exp(iq_z z_m)\right|^2, \quad (4)$$

where $\sigma=\sigma_0=\sigma_1=\sigma_2$, z_m are the locations of the interfaces, $\rho_0=0$, the other ρ_m are the electron densities of the layers, and the σ_m parameters determine the interfacial width between the slabs of electron density (the standard deviation of their locations, z_m).

Overall, fitting the experimental data at $q_z>0.1$ Å^{-1} either using Parratt formalism or the first Born approximation gives fits with similar quality for layers 1 and 2 (ρ_1, ρ_2, ρ_3, l_1, l_2, and σ) that are the same within the error bars of the parameters. I generated the solid lines in Fig. 3 using Eq. (4) with the parameters listed in Table I; they illustrate the changes in the surface-normal structure after doping the hydrosols with different alkali ions. The density ρ_1 is the only parameter of the surface-normal structure that depends strongly on the composition of the alkali metal. It is noticeably smaller than ρ_b and is determined by the Z-number, Z^+ of the dopant. In contrast, the thicknesses, l_1 and l_2, and the densities, ρ_2 and ρ_3, are dependent minimally on the alkali-metal composition of the sol. I note that the estimated density of the depleted region, ρ_3, is close to the electron density of water, ρ_w. σ coincides within the error bar with the width of the capillary wave $\sigma_{cap}=2.7\pm0.2$ Å, that is given by the resolution of the detector $q_z^{max}\approx0.7$ Å^{-1}, and a short wavelength cutoff in the spectrum of the capillary waves: $\sigma_{cap}^2 \approx k_B T \ln(Q_{max}/Q_{min})/(2\pi\gamma)$, where $Q_{min}=q_z^{max}\Delta\beta/2$ and $Q_{max}=2\pi/a$ ($a\approx3$ Å is close to the intermolecular distance). The tension at the surfaces of the sols, $\gamma \approx 69-74$ dyn/cm, was measured by a Wilhelmy plate. These results also agree well with the data reported in Ref. 34 for sols with much smaller particles.

Figure 4(a) depicts the model distributions of electron density $\rho_1(z)$ in layer 1.[47] Figure 4(b) illustrates the dependence of the integral electron densities of this layer 1, $\Gamma_1(\sim\rho_1 l_1)$, as a function of Z^+, where the circles and squares, respectively, correspond to the x-ray reflectivity data in Fig. 3 and in Ref. 34. The solid line in Fig. 4(b) is a linear fit of all points. The slope of the line, Θ, is the surface density of alkali ions in layer 1 $\Theta\approx4\times10^{18}$ m^{-2} since $\Theta=d\Gamma_1/dZ^+\approx(\Gamma_1^M-\Gamma_1^{Na})/(Z_M^+-Z_{Na}^+)$, where $Z_{Cs}^+=54$, $Z_{Rb}^+=36$, $Z_K^+=18$, and $Z_{Na}^+=10$, correspondingly, are the numbers of electrons in Cs^+, Rb^+, K^+, and Na^+. Accordingly, for the Cs- and Rb-enriched sols, the electron density of layer 1 is due to the suspended alkali ions. However, $\Gamma_1\approx2\times10^{19}$ m^{-2} when $Z^+\to0$ (constant term) so that either the alkali ions with small Z^+s adsorb in layer 1 with the density Θ 50% higher than heavy ions or the composition of the layer is more complex. For example, there could be one H_2O molecule per two alkali ions in the layer (H_2O contains ten electrons). Indeed, the former suggestion is in the excellent agreement with the grazing-incidence diffraction data: At pH=9, the surface density of Na^+ is as high as $\Theta_{Na}\approx6\times10^{18}-7\times10^{18}$ m^{-2}.[34,35]

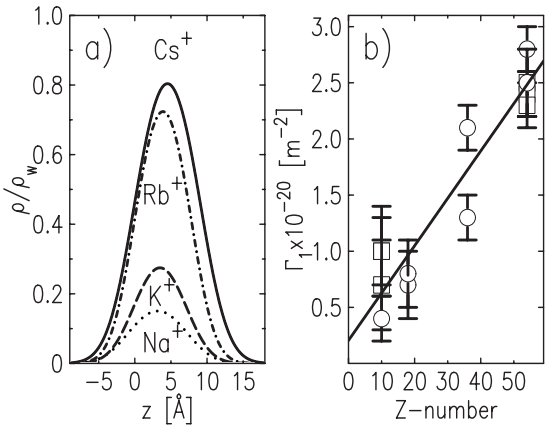

FIG. 4. (a) Model distributions of electron density $\rho_1(z)$ in layer 1, normalized to the density of bulk water. (b) Integral density of layer 1 vs the number of electrons in the alkali ion, where $Z_{Cs}^+=54$, $Z_{Rb}^+=36$, $Z_K^+=18$, and $Z_{Na}^+=10$, respectively, are the numbers of electrons in Cs^+, Rb^+, K^+, and Na^+. The circles and squares correspond to the reflectivity curves in Fig. 3 and the data obtained from Ref. 34, respectively. A solid line is the linear fit of these data.

The same size effect as in layer 1 is apparent at the surface of the sol enriched by both K^+ and Cs^+ ions. Since Cs^+ is noticeably larger than K^+, the former should replace the latter in layer 1 for the same reason that Cs^+ (or K^+) replaces Na^+. The stars and crosses in Fig. 3 correspond, respectively, to the surface-structure factors of hydrosols containing ~0.3 mol/l of Cs and ~0.4 mol/l of K. The estimated integral density of layer 1 of the twice-doped sols is as high as $\Gamma_1\approx2\times10^{20}$ m^{-2} ($\rho_1\approx0.8\rho_w$ and $l_1\approx8$ Å). Then, the content of K^+ in layer 1, $x\approx0.1$ [easily established by solving the following linear equation: $Z_K^+x+Z_{Cs}^+(1-x)=\Gamma_1/\Theta$], is in quantitative agreement with the Ultrup–Kharkats theory.

Thus, the variation in surface-normal structures of the hydrosols enriched by different alkali metals can be related to the ion-size effect in layer 1: Larger ions (for example, Cs^+) selectively accumulate in this layer by replacing smaller ions (such as Na^+ and K^+). However, the estimated center of the layer 1 lies ~4 Å above the surface of the sol. It is twice as large as the position of the minimum in Fig. 1(b). Although the slab model applied in this work was adequate for the spatial resolution of the x-ray reflectivity experiment, $2\pi/q_z^{max}\sim10$ Å, it does not afford information at atomic resolution about the true distribution of the ions. Thus, increasing the number of layers and/or number of fitting parameters hardly improved the quality of the fits. A quantitative interfacial model is required that would account for the inhomogeneous spatial distribution of ions along the z-axis, for example, to make a meaningful comparison between the experimental findings and the Kharkats–Ulstrup theory.

The author would like to acknowledge Anna I. Lygina, Vladimir I. Marchenko, Vitalii V. Zavialov, and Avril Woodhead for valuable discussions and their comments on the

manuscript. Beamline X19C received support from the ChemMatCARS National Synchrotron Resource, the University of Chicago, the University of Illinois at Chicago, and Stony Brook University. Use of the National Synchrotron Light Source, Brookhaven National Laboratory, was supported by the U.S. Department of Energy, Office of Science, Office of Basic Energy Sciences, under Contract No. DE-AC02-98CH10886. The author also thanks Grace Davison for providing Ludox solutions of colloidal silica.

[1] A. W. Adamson, *Physical Chemistry of Surfaces*, 3rd ed. (Wiley, New York, 1976).
[2] P. Becher, *Emulsions: Theory and Practice*, 3rd ed. (American Chemical Society, Washington, D.C./Oxford University Press, Oxford, 2001).
[3] A. Yu. Grosberg, T. T. Nguyen, and B. I. Shklovskii, Rev. Mod. Phys. **74**, 329 (2002).
[4] G. Gouy, J. Phys. **9**, 457 (1910).
[5] D. L. Chapman, Philos. Mag. **25**, 475 (1913).
[6] E. J. W. Verwey and K. F. Nielsen, Philos. Mag. **28**, 435 (1935).
[7] O. Stern, Z. Elektrochem. **30**, 508 (1924).
[8] C. Wagner, Phys. Z. **25**, 474 (1924).
[9] L. Onsager and N. N. T. Samaras, J. Chem. Phys. **2**, 528 (1934).
[10] Y. I. Kharkats and J. J. Ulstrup, Electroanal. Chem. **308**, 17 (1991).
[11] M. A. Vorotyntsev, Yu. A. Ermakov, V. S. Markin, and A. A. Rubashkin, Russ. J. Electrochem. **29**, 730 (1993).
[12] A. G. Volkov, D. W. Dreamer, D. L. Tanelli, and V. S. Markin, Prog. Surf. Sci. **53**, 1 (1996).
[13] Y. Levin, J. Chem. Phys. **113**, 9722 (2000).
[14] V. S. Markin and A. G. Volkov, J. Phys. Chem. B **106**, 11810 (2002).
[15] J. Zwanikken and R. van Roij, Phys. Rev. Lett. **99**, 178301 (2007).
[16] I. Benjamin, Chem. Rev. (Washington, D.C.) **96**, 1449 (1996).
[17] P. Jungwirth and D. J. Tobias, Chem. Rev. (Washington, D.C.) **106**, 1259 (2006).
[18] T. M. Chang and L. X. Dang, Chem. Rev. (Washington, D.C.) **106**, 1305 (2006).
[19] K. Kjaer, J. Als-Nielsen, C. Helm, P. Tippman-Krayer, and H. Möhwald, J. Phys. Chem. **93**, 3200 (1989).
[20] M. J. Bedzyk, G. M. Bommarito, M. Caffrey, and T. L. Penner, Science **248**, 52 (1990).
[21] V. M. Kaganer, H. Möhwald, and P. Dutta, Rev. Mod. Phys. **71**, 779 (1999).
[22] J. Daillant and M. Alba, Rep. Prog. Phys. **63**, 1725 (2000).
[23] D. Vaknin, P. Krüger, and M. Lösche, Phys. Rev. Lett. **90**, 178102 (2003).
[24] K. Besteman, M. A. G. Zevenbergen, H. A. Heering, and S. G. Lemay, Phys. Rev. Lett. **93**, 170802 (2004).
[25] W. Bu, D. Vaknin and A. Travesset, Phys. Rev. E **72**, 060501(R) (2005).
[26] C. Park, P. A. Fenter, N. C. Sturchio, and J. R. Regalbuto, Phys. Rev. Lett. **94**, 076104 (2005).
[27] G. Luo, S. Malkova, J. Yoon, D. G. Schultz, B. Lin, M. Meron, I. Benjamin, P. Vanysek, and M. L. Schlossman, Science **311**, 216 (2006).
[28] E. Sloutskin, J. Baumert, B. M. Ocko, I. Kuzmenko, A. Checco, L. Tamam, E. Ofer, T. Gog, and M. Deutsch, J. Chem. Phys. **126**, 054704 (2007).
[29] M. L. Schlossman and A. M. Tikhonov, Annu. Rev. Phys. Chem. **59**, 153 (2008).
[30] B. S. Gourary and F. S. Adrian, Solid State Phys. **10**, 127 (1960).
[31] J. E. Huheey, E. A. Keiter, and R. L. Keiter, *Inorganic Chemistry: Principles of Structure and Reactivity*, 4th ed. (Harper Collins, New York, 1993).
[32] A. M. Tikhonov, J. Phys. Chem. B **110**, 2746 (2006).
[33] A. M. Tikhonov, J. Chem. Phys. **124**, 164704 (2006).
[34] A. M. Tikhonov, J. Phys. Chem. C **111**, 930 (2007).
[35] A. M. Tikhonov, J. Chem. Phys. **126**, 171102 (2007).
[36] I. Danielewicz-Ferchmin and A. R. Ferchmin, J. Phys. Chem. **100**, 17281 (1996).
[37] Solid KOH, $RbOH \cdot H_2O$, and $CsOH \cdot H_2O$ (99.95% on metal basis) were obtained from Sigma-Aldrich. Grace Davidson kindly supplied the monodispersed silica hydrosol of 22 nm particles Ludox TM-50 (~50% of SiO_2 and ~0.2% of Na by weight) that was further dissolved in de-ionized water to form the sol containing ~30% of SiO_2 (by weight).
[38] The solubility of Li^+ and Na^+ in the silica hydrosols is limited to ~0.15 mol/l since they cause the sols to coagulate at $pH > 11$, whereas K^+, Rb^+, Cs^+ cations are ineffective, and remain so even at much higher bulk concentrations; J. Depasse and A. Watillon, J. Colloid Interface Sci. **33**, 430 (1970).
[39] M. L. Schlossman, D. Synal, Y. Guan, M. Meron, G. Shea-McCarthy, Z. Huang, A. Acero, S. M. Williams, S. A. Rice, and P. J. Viccaro, Rev. Sci. Instrum. **68**, 4372 (1997).
[40] L. G. Parratt, Phys. Rev. **95**, 359 (1954).
[41] J. Als-Nielsen, *Topics in Current Physics, Structure and Dynamics of Surfaces* (Springer-Verlag, Berlin, 1986), Vol. 2.
[42] P. S. Pershan, Faraday Discuss. Chem. Soc. **89**, 231 (1990).
[43] F. P. Buff, R. A. Lovett, and F. H. Stillinger, Phys. Rev. Lett. **15**, 621 (1965).
[44] J. Daillant, L. Bosio, B. Harzallah, and J. J. Benattar, J. Phys. II **1**, 149 (1991).
[45] D. K. Schwartz, M. L. Schlossman, E. H. Kawamoto, G. J. Kellogg, P. S. Pershan, and B. M. Ocko, Phys. Rev. A **41**, 5687 (1990).
[46] A. Braslau, P. S. Pershan, G. Swislow, B. M. Ocko, and J. Als-Nielsen, Phys. Rev. A **38**, 2457 (1988).
[47] The distribution of the electron density in the layer 1 can be obtained from the model's electron-density profile $\rho(z) \approx \frac{1}{2}\rho_3 + \frac{1}{2}\Sigma_{m=0}^{2}(\rho_{m+1} - \rho_m)\mathrm{erf}(t_m(z)/\sigma_m\sqrt{2})$, $t_m(z) = z + \Sigma_{i=0}^{m} z_i$, and $\mathrm{erf}(t) = (2/\sqrt{\pi})\int_0^t e^{-s^2} ds$ by subtracting from it the contributions of layers 2–3 and the hydrosol's bulk.